H.-M. Bauschke, D. T. Read†, and K.-H. Schwalbe**

Crack Growth Resistance at Surface Cracks in Three Aluminium Alloys

REFERENCE Bauschke, H.-H., Read, D. T., and Schwalbe, K.-H., **Crack growth resistance at surface cracks in three aluminium alloys**, *Defect Assessment in Components – Fundamentals and Applications*, ESIS/EGF9 (Edited by J. G. Blauel and K.-H. Schwalbe) 1991, Mechanical Engineering Publications, London, pp. 749–764.

ABSTRACT This paper is a part of an extensive study which concerns the transferability of critical values of selected fracture correlation parameters of standard fracture mechanics specimens to surface crack tensile panels. Two high-strength aluminium alloys, Al 7075-T7351 and Al 2024-T351, and Al 2024-FC (furnace cooled), an over-aged material with low yield strength and high strain hardening coefficient, were tested. An important element of the paper is the estimation of J integral values for the surface crack tensile panels by an approximation method presented in this work.

The final (Δ_a, J) values of tensile panels with different surface cracks were compared with the CT and SENB specimen R curve data of the same material. For the two high strength aluminium alloys the surface crack data were higher than the CT and SENB specimen data by a factor of about 3 in the J integral. In contrast, for Al 2024-FC the surface crack data were close to the testpiece R curves. The results show that a prediction of the crack growth properties of three-dimensional configurations by simply using the J–R curves of standard laboratory specimens is problematical.

Introduction

Fracture mechanics normally considers through-cracks whose crack fronts are straight and perpendicular to the surface, although in many technical structures surface cracks are much more prevalent (1). Because experiments as well as calculations on specimens with surface cracks are very time-consuming, owing to the three-dimensional crack shape, attempts are being made to transfer characteristic values as determined by fracture mechanics on standard through-crack specimens first to specimens with surface cracks and finally to components with surface cracks. This transferability concept is currently the subject of intensive investigations because, with an understanding of the superimposed mechanisms and relationships, fracture mechanics estimates of the service life of structures can be done much more exactly than is nowadays normally the case.

This paper investigates the transferability of fracture mechanics properties from standard specimens (CT, SENB) to tension plates with a central surface crack in the elastic–plastic regime including stable crack growth. The J integral was selected as the loading parameter, as it is most commonly used in elastic–plastic fracture mechanics.

* Institut für Werkstofforschung, GKSS-Forschungszentrum Geesthacht GmbH, 2054 Geesthacht, FRG.

† United State Department of Commerce, National Institute of Standards and Technology, Fracture and Deformation Division, Boulder, Colorado 80303-3328, USA.

For standard fracture mechanics specimens, experimental determination of the J integral is standardised (e.g., **(2)**) whereas for surface crack tension plates, a precise determination is only possible by numerical calculations.

Because the authors had no access to FE calculations, the J values at the surface cracks were determined by a simple approximation method presented in this paper.

Besides the comparison of J–R curves of CT and SENB specimens with J–Δa data of surface crack tension specimens, fractographic observations are an important element of this work.

Experimental

Three aluminium alloys were examined. Tensile properties are listed in Table 1. Two of the alloys, Al 2024-T351 and Al 7075-T7351, are high-strength alloys commonly used in aerospace applications.

Al 2024-FC is Al 2024-T351 in a furnace cooled condition, which has a low yield strength and high work hardening exponent.

The J–R curves of the materials were determined by CT and SENB specimens according to ASTM E813-81 **(2)**. The surface crack tension plates were 10 mm thick, 100 mm wide, and 500 mm long (Fig. 1). The surface cracks were machined by spark erosion and were allowed to grow by fatigue in tension and/or bending to different end shapes, which can be characterised by the parameters a/t and a/c (Table 2).

For the tension tests with monotonically rising load, the specimens were instrumented with different displacement and strain transducers described elsewhere **(3)**. For this paper, only the measurement of CMOD (crack mouth opening displacement) determined over a measurement base of 2.5 mm to either side of the crack plane (Fig. 1) was relevant. The specimens were tested in displacement control. After a specific amount of stable crack growth which could be estimated by the DC potential drop method, the current crack front was marked by fatigue cracking (Fig. 2).

After marking, the tension test was continued and up to four further markings were made.

Table 1 Tensile properties of the three aluminium alloys used in this study. All specimens are in the longitudinal orientation

Material	*Yield strength* σ_{Ys} *(N/mm²)*	*Ultimate strength* σ_u *(N/mm²)*	*Elongation (percent)*	*Reduction of area (percent)*	*Plate thickness (mm)*
Al 7075-T7351	429	504	13	26	32
Al 2024-T351	360	468	20	20	132
Al 2024-FC*	82	220	18	28	132

* Al 2024-T351 with heat treatment 2 h 410°C – 30°/h – 250°C – air

Table 2 Relative crack sizes, experimental results and calculated J values for the surface-cracked tensile panels. The angle ϕ^* is the value of the parametric angle, corresponding to the location of maximum crack extension

Specimen	a/t	a/c	$CMOD_{pl}$ *(mm)*	ϕ^* *(degrees)*	Δa (ϕ^*) *(mm)*	J_{el} $(\phi = 90$ *degrees)* *(N/mm)*	J_{pl} $(\phi = 90$ *degrees)* *(N/mm)*	$\frac{J(\phi = 25\text{degrees})}{J(\phi = 90\text{ degrees})}$	J $(\phi = 25$ *degrees)* *(N/mm)*
Al 7075-T7351									
21010	0.29	1.10	0.32	33	0.28	12.3	138	1.0	150
22010	0.46	0.85	0.21	30	0.31	23.8	99	1.0	123
23010	0.75	0.74	0.42	28	1.00	45.4	182	1.1	250
24010	0.47	0.46	0.36	20	0.65	45.9	174	0.7	154
25010	0.63	0.41	0.46	20	1.65	68.3	224	0.9	263
Al 2024-T351									
11010	0.50	0.97	0.033	35	0.10	12	22.7	1.0	34.7
13010	0.54	1.07	0.10	30	0.39	13.2	44.2	1.0	57.4
Al 2024-FC									
1F1010	0.50	1.06	0.31	20	0.88	2.5	39	1.0	41.5
1F2010	0.47	0.87	1.01	22	3.28	5.5	127	1.0	133
1F3010	0.47	0.98	0.72	30	1.49	4.6	91	1.0	95.6

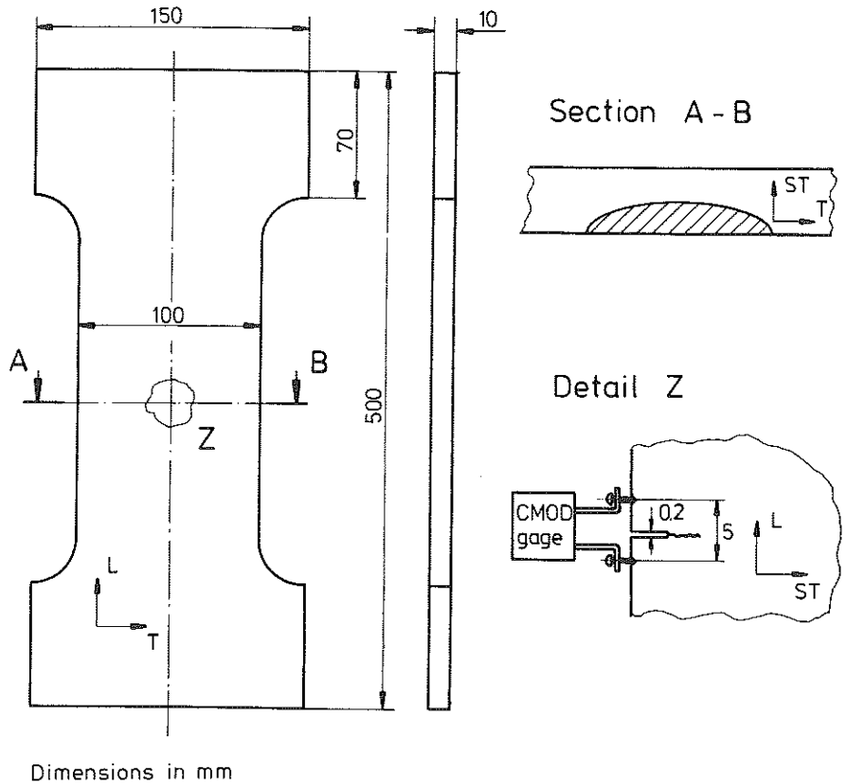

Fig 1 Surface crack tensile panel with CMOD gauge

Estimation method for *J* integral of surface crack tension specimens

The *J* integral can be determined under small scale yielding conditions by

$$J = m\sigma_y \mathrm{CTOD} \tag{1}$$

where

m = constraint factor
σ_y = effective flow stress
CTOD = crack tip opening displacement

Under certain conditions, this equation relating *J* and CTOD is thought to hold also for elastic–plastic material behaviour **(4)**. The constraint factor m has been studied in numerous papers (e.g., **(5)**–**(7)**) and is dependent on specimen geometry, stress condition, and work-hardening exponent. It is assumed that *J* consists of an elastic and plastic part

$$J = J_{el} + J_{pl} \tag{2}$$

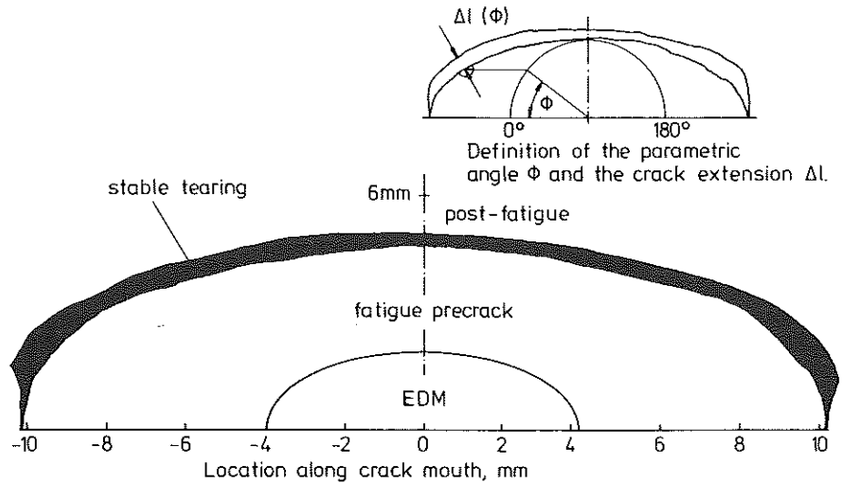

Fig 2 Fracture surface of a surface crack tensile panel showing the electrical-discharge-machined notch, the fatigue precrack, and a zone of stable tearing followed by post-fatigue

where

$$J_{el} = \frac{K^2}{E(1-\nu^2)} \tag{3}$$

K = linear elastic stress intensity factor **(8)**
E = Young's modulus
ν = Poisson ratio

$$J_{pl} = m\sigma_y \mathrm{CTOD}_{pl} \tag{4}$$

It is assumed that by using a crack opening factor X_{op} = CTOD/CMOD from the extrapolation method, CTOD_{pl} at the deepest point of the crack (ϕ = 90 degrees) can be approximately determined. In two FE studies (**(9)(10)**, Table 3) X_{op} values from surface cracks of different a/t ratios have been deter-

Table 3 Ratio *J* (ϕ = 25 degrees) to *J* (ϕ = 90 degrees), ratio X_{op} = CTOD/CMOD and constraint factor $m = J/(\sigma_y \mathrm{CTOD})$; from finite element calculations (9)–(13)

Reference	a/t	a/c	J (ϕ = 25 degrees) / J (ϕ = 90 degrees)	X_{op}	m
(12)	0.1	0.7	0.84	—	—
(13)	0.25	0.33	0.50	—	—
(13)	0.25	0.50	0.77	—	—
(13)	0.25	0.67	0.87	—	—
(9)	0.27	0.58	0.59	0.59	1.50
(11)	0.55	0.24	0.73	—	1.48
(10)	0.65	0.65	1.09	0.51	1.44

mined. A straight line was drawn through a plot of these X_{op} versus a/t values, and the X_{op} values of the specimens used in this study were determined according to their a/t values.

The constraint-factor m was taken from the average of the values of three FE studies of surface crack tension plates **(9)–(11)**. All three values were about 1.5 (Table 3).

For the effective yield stress of the two high-strength materials, which essentially show elastic–ideal plastic behaviour, the average of the yield stress $R_{p0.2}$ and maximum stress R_m was taken. The same procedure was used for the high-hardening material, Al 2024-FC. The J values were calculated not at $\phi = 90$ degrees, but at the point of maximum stable crack growth, which was at about $\phi = 25$ degrees (Table 2), assuming a further elliptical crack front.

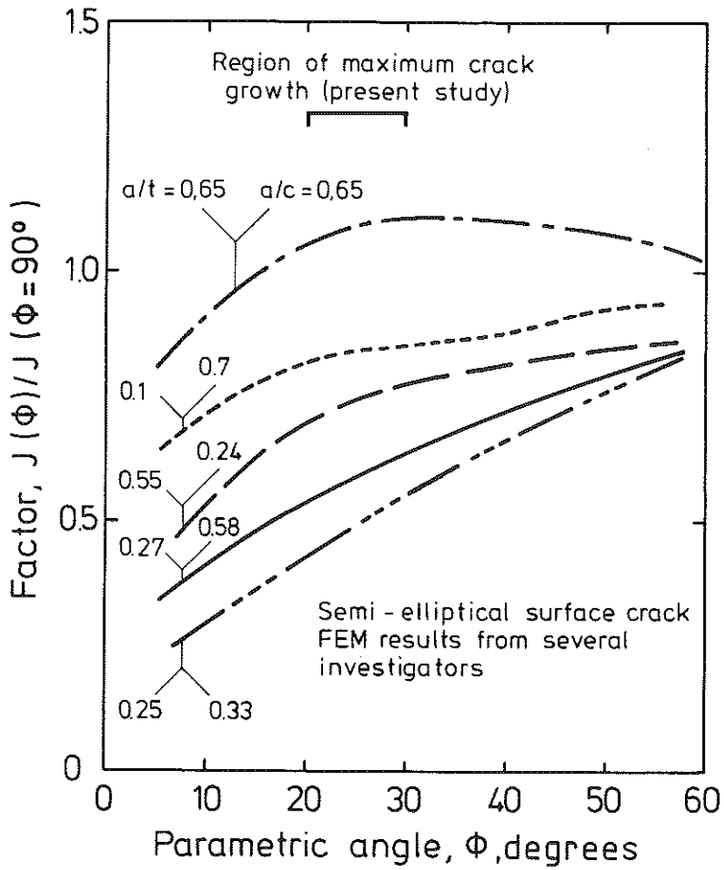

Fig 3 Finite element results collected from the literature for the variability of the J integral along a surface crack front

Because the J integral level over the crack contour at a given load varies greatly and also depends on the crack shape, the ratio $J_{25\ degrees}/J_{90\ degrees}$ also had to be determined. Fig. 3 shows $J_\phi/J_{90\ degrees}$ plotted against ϕ from five FE studies **(9)–(13)**. The $J_{25\ degrees}/J_{90\ degrees}$ values were taken from this figure and replotted in an a/c versus a/t diagram, from which the desired $J_{25\ degrees}/J_{90\ degrees}$ values of the tested panels were assessed.

Results

J–R *curves*

The J–R curves measured on standard specimens containing through-cracks are shown in Figs 4, 6, and 7. The R curves of L–LT and L–ST oriented specimens are very similar.

The higher constraint of the side-grooved specimens leads to somewhat lower resistance against crack growth. The same is true for greater specimen thickness.

The J–Δa curves of standard specimens of Al 7075-T7351 are higher than those out of Al 2024-T351. It shall be pointed out in this context that the J–R

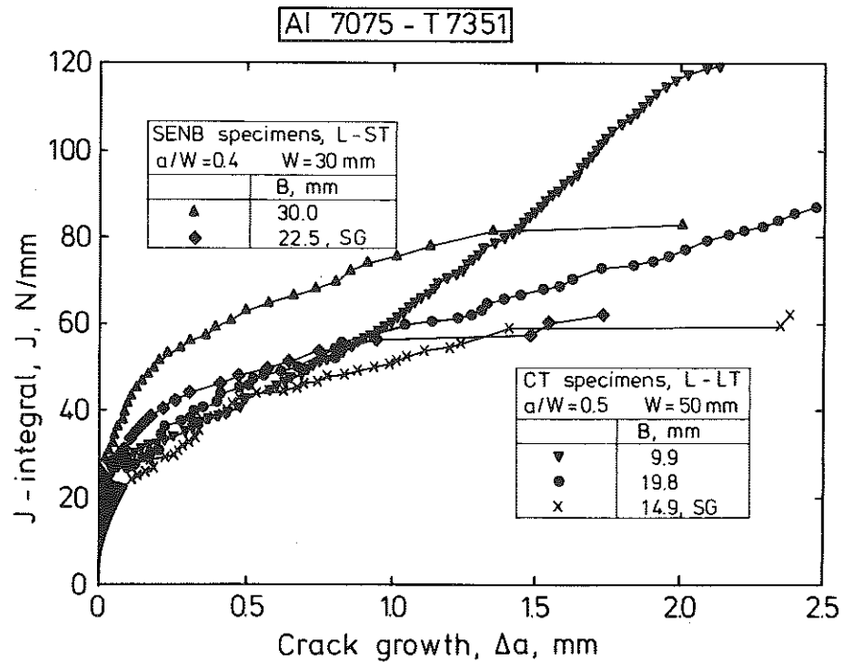

Fig 4 J–R curves from CT and SENB specimens of Al 7075-T7351, including specimens in thicknesses as indicated, in the L–T and L–ST orientations

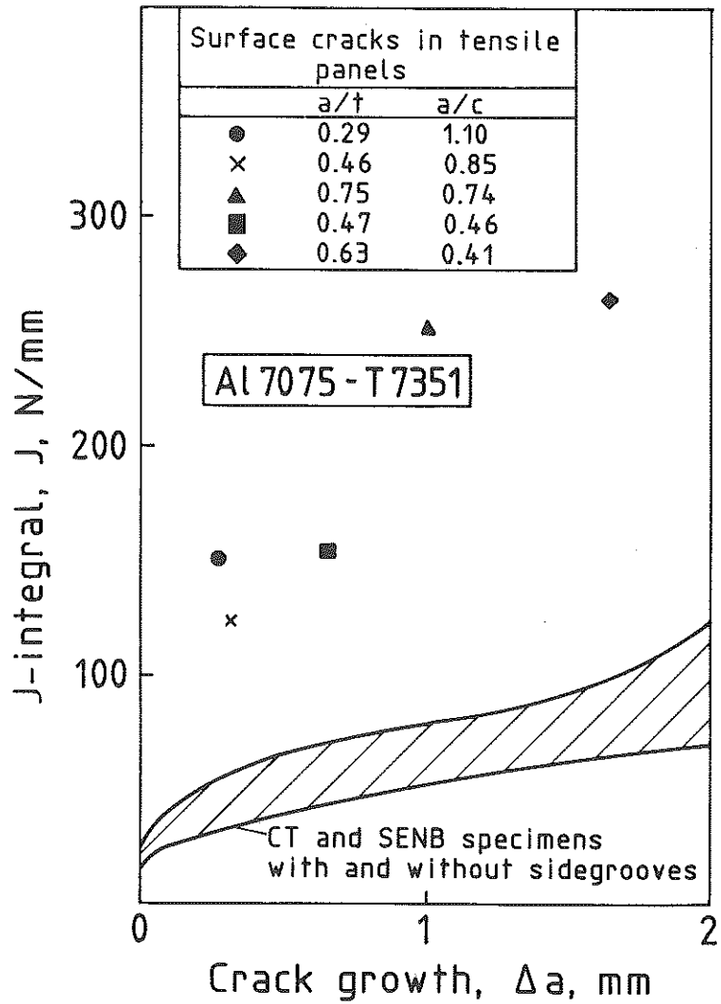

Fig 5 ***J*** **integral values from surface crack tensile panels plotted for comparison with the CT and SENB specimen** ***J–R*** **curves for the high strength aluminium alloy Al 7075-T7351**

behaviour of high strength aluminium alloys seems to depend strongly on the charge of the material. Hellmann **(14)** obtained J–Δa curves from comparable specimens of another charge of Al 2024-T351, which were clearly above those shown here for Al 7075-T7351.

In Fig. 5, the J–Δa values at the point of maximum crack growth of the surface cracks in Al 7075-T7351 are plotted into the scatter band from Fig. 4. The J values for surface crack data points are by a factor of roughly 3 higher than those for the standard specimens. The other high strength aluminium

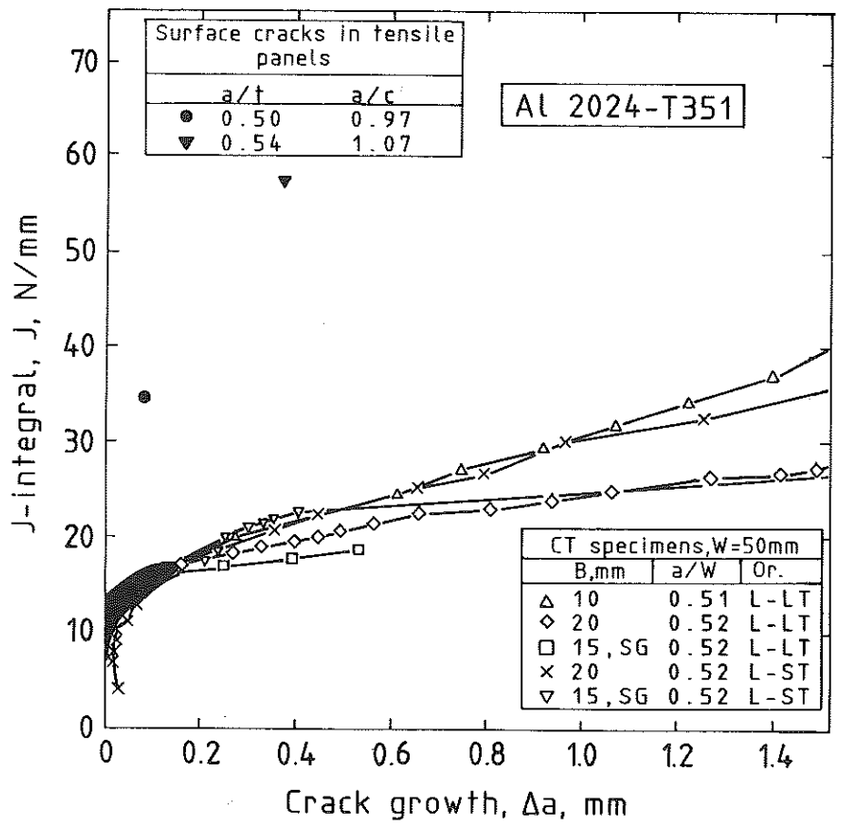

Fig 6 ***J*** **integral values from surface crack tensile panels plotted for comparison with the testpiece** ***J–R*** **curves for the high strength alloy Al 2024-T351**

alloy, Al 2024-T351, shows similar results (Fig. 6). In contrast, the Al 2024-FC surface crack values nearly fall into the J–Δa scatter band of the CT specimens (Fig. 7).

Fractographic observations

For a better understanding of the above results concerning stable tearing at different specimen geometries, it is instructive to report some fractographic observations. Figure 8 shows the percentage of shear lip thickness for 10 mm thick CT specimens from the beginning of stable tearing for the three materials tested. The shear lips in Al 7075-T7351 and Al 2024-FC occupy most of the specimen thickness after a few millimetres, whereas in Al 2024-T351, the shear lips cover only about 10 percent of the specimen thickness. The observations from the fracture surfaces of the surface crack tension plates show the same tendency, as sketched in Figs 9 and 10.

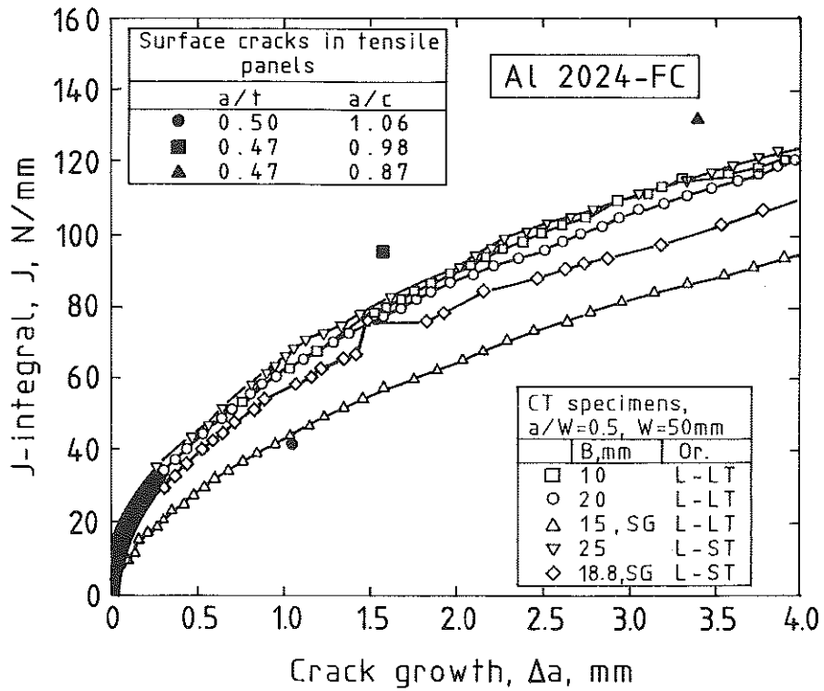

Fig 7 ***J*** **integral values from surface crack tensile panels plotted for comparison with the testpiece *J–R* curves for the soft aluminium alloy Al 2024-FC (furnace-cooled)**

(1) The amount of stable crack growth for about the same starter crack ($a/t \approx 0.5$, $a/c \approx 1.0$) is very different: in Al 2024-FC the stable tearing continues until far beyond the break-through of the crack through the back surface (Fig. 9(a)), whereas in Al 2024-T351 only very limited stable crack growth is seen, about 0.7–1.5 mm, depending on the location along the crack front (Fig. 9(b)). Al 7075-T7351 exhibits intermediate behaviour with about 2–6 mm stable tearing (Fig. 10(b)). For small surface cracks, the stable crack growth increases in comparison to the original crack length and depth, whereas it clearly decreases for larger cracks (Fig. 10(a) and (c)).

(2) As in the CT specimens (Fig. 8), the surface-crack tension specimens of Al 2024-T351 show very little shear fracture, whereas the shear fracture areas in Al 2024-FC and Al 7075-T7351 are roughly the same and comparable. Shear fracture begins at the so-called leading edges of the surface crack ($\phi = 0$ degrees), indicating the prevailing plane stress conditions.

(3) The normal fracture plane extends furthest at an angle ϕ^*, which coincides with the maximum of stable crack growth along the crack contour. This indicates that the largest constraint over the crack contour occurs at this angle.

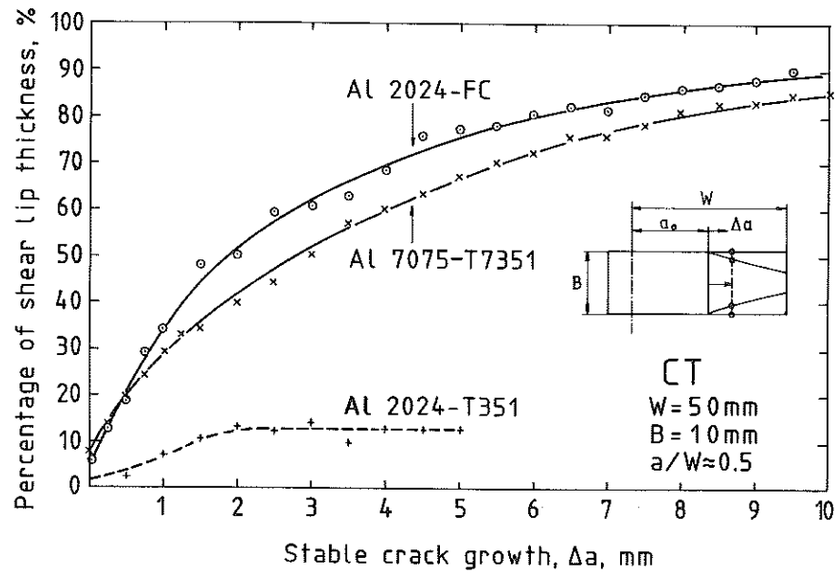

Fig 8 Percentage of shear lip thickness for 10 mm thick CT specimens from the beginning of stable tearing for the three materials tested

In Fig. 11, the stable tearing until the first marking in the five surface crack tension plates of Al 7075-T7351 is plotted against the angle ϕ. A maximum at $\phi \approx 25$ degrees can clearly be seen.

Discussion

The most striking result is not only that there are differences in the *J–R* curve behaviour between CT specimens and surface cracks but that different materials respond in such a different manner to a variation of specimen geometry. In the case of the two high strength alloys the surface cracks under tension produced a much higher resistance against crack growth than the through-cracks under bending, whereas the low strength material exhibited always the same crack growth resistance.

Uncertainties in the J determination of the surface cracks through uncertainties in m, X_{op}, and $J_\phi/J_{90\ degrees}$ have of course to be accounted for. But they are not believed to alter the observed trends.

As the authors had no access to three-dimensional finite element calculations, the following discussion will be conducted on qualitative arguments considering the constraint in the specimens. It is anticipated that constraint is gradually reduced when a specimen is deformed up into fully plastic conditions.

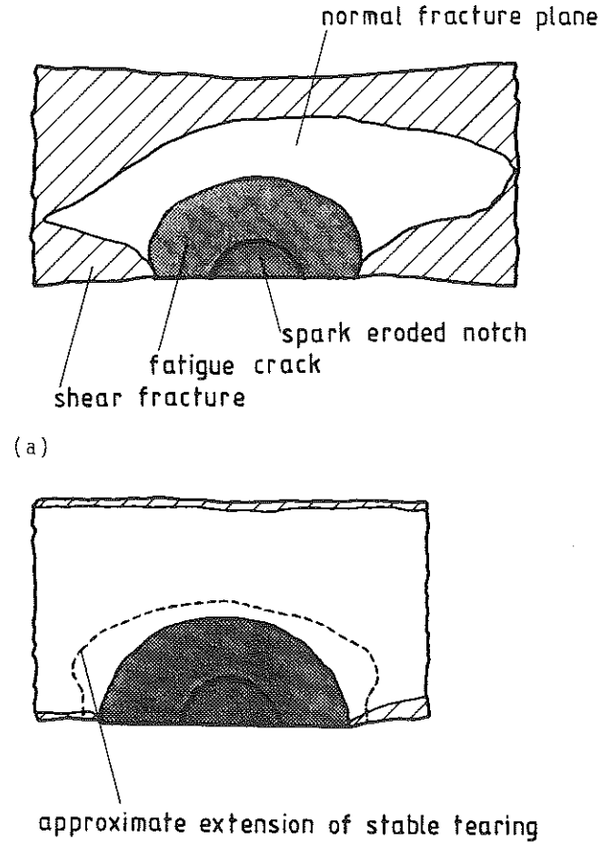

Fig 9 Observations from fracture surfaces of surface crack tensile panels: (a) Al 2024-FC, $a/t = 0.50$, $a/c = 1.07$; (b) Al 2024-T351, $a/t = 0.48$, $a/c = 0.95$

It should be borne in mind that the R curves from the surface cracks were determined as local R curves at an angle of $\Phi \approx 25$ degrees where probably the highest constraint is effective **(15)** and thus the lowest crack growth resistance should be present. If average J–R curves had been determined as in the case of the CT specimens the difference for the high strength materials between surface cracks and CT specimens would be even greater. On the other hand, if local R curves had been determined in the centre of the CT specimens (where the highest constraint occurs) those curves had been flatter than the actually determined ones, thus increasing the difference even more.

An important information for fracture mechanics analyses is the location of the loading state with respect to the yield load, F_y, expressed, e.g., in terms of the applied load, F, normalised by the yield load, F/F_y. Table 4 shows these

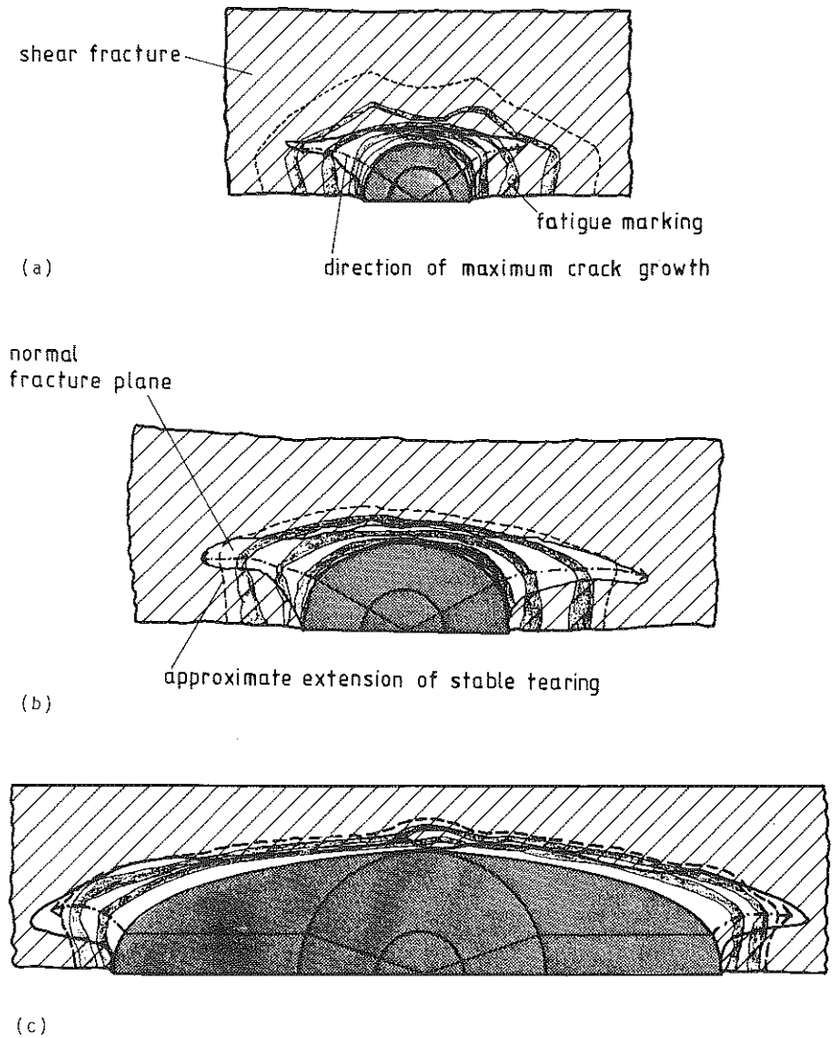

Fig 10 Observations from fracture surfaces of surface crack tensile panels of Al 7075-T7351 with different surface cracks: (a) $a/t = 0.29$, $a/c = 1.10$; (b) $a/t = 0.46$, $a/c = 0.85$; (c) $a/t = 0.63$, $a/c = 0.41$ (compare with Fig. 10)

normalised loads for crack initiation and maximum load conditions for the two specimen geometries and the three materials. Whilst crack initiation in the CT specimens of the high strength material occurs at about one half of F_y, it is observed to take place around limit load in the low strength material. However, initiation at surface cracks takes place at about yield load for all

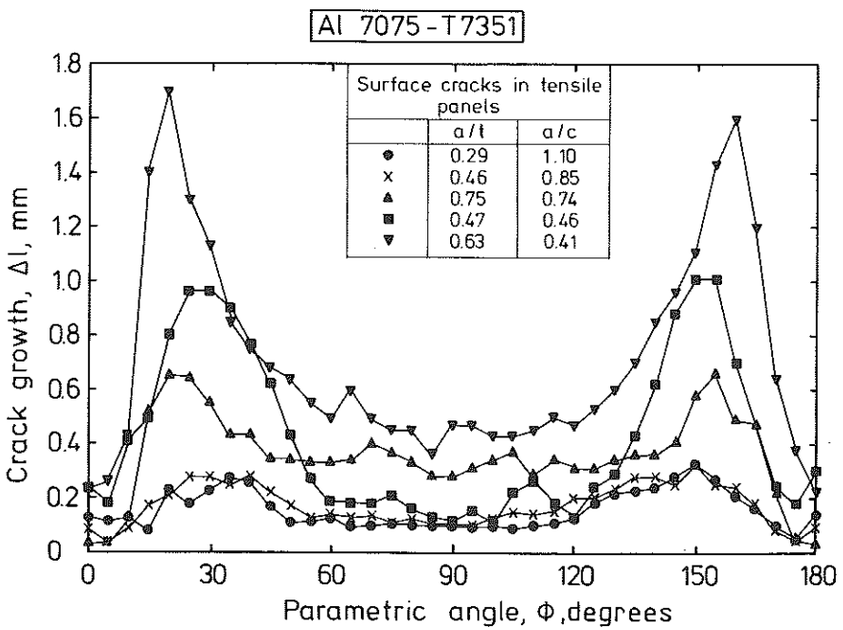

Fig 11 Stable tearing until the first marking along the front of the five surface crack tension plates of Al 7075-T7351 as a function of the parametric angle ϕ

three materials. From the foregoing it is concluded that in the high strength materials constraint is substantially reduced in the surface crack tension configuration as compared with CT specimens of the same thickness, thus contributing to the increase of crack growth resistance.

In the low strength material, the level of F/F_y at initiation minimises the difference in constraint between the different specimen types tested, thus giving rise to comparable crack growth resistance. The relatively configuration inde-

Table 4 Applied load at crack initiation F_i and maximum load F_{max} normalised by the limit load F_y for surface crack tensile specimens (SCT) and CT specimens for all materials

Material	W = *50 mm* CT B = *10, 25 mm* (*partly 25% side-grooved* a/W ≈ *0.5*		W = *50 mm* SCT t = *10 mm* a/t ≈ *0.5* a/c ≈ *1.0*	
	F_i/F_y*	F_{max}/F_y*	F_i/F_y	F_{max}/F_y
Al 7075-T7351	0.45–0.55	0.76–0.81	≈1.0	≈1.07
Al 2024-T351	0.40–0.50	0.53–0.63	≈0.9	≈1.0
Al 2024-FC	1.0–1.3	1.7–2.1	≈1.0	≈2.4

* F_y for CT specimens is calculated assuming plane stress

pendent crack growth resistance of Al 2024-FC has also been reported by Heerens **(16)**.

The reduction in constraint at surface cracks is variable along the crack front; it is most pronounced near the leading edge and at the deepest point of the crack **(15)**. Several investigators **(17)–(20)** showed that the behaviour of stable crack growth at three-dimensional crack configurations can be explained by the variation of constraint along the crack front. These findings and the present work show that the prediction of the crack growth properties of three-dimensional crack configurations cannot be performed in a one-parameter fashion, i.e., by simply using an R curve of a standard specimen, whereas conservative assessments seem to be possible from the present results. However, this is not necessarily true for other configurations, like surface cracked plates under biaxial bending **(21)**.

This discussion shows that a quantification of constraint conditions and knowledge about the material dependent response to constraint variation are vital for solving the transferability problem.

Summary

The subject of this paper is the question of transferability of available J–R curves from simple laboratory specimens (CT, SENB) to specimens more similar to components, in this case surface crack tension plates. A simple approximation procedure to calculate J integral values of surface crack tension plates is introduced. Tests were done on two high-strength aluminium alloys, Al 2024-T351 and Al 7075-T7351, and on the furnace-cooled alloy Al 2024-FC. The comparison of the J–R curves of laboratory specimens with J values calculated at the point of maximum crack growth at the crack contour of surface cracks shows, that the surface crack J–Δa values of the two high-strength aluminium alloys fall well above the J–R scatter bands of the simple laboratory specimens. However, the surface face crack J–Δa values of the furnace cooled aluminium-alloy fall roughly within the J–R scatter band of the standard specimens. The results, complemented by fractographic observations, show that a transfer of the J–R curves of simple laboratory specimens to structures with three-dimensional cracks is problematical.

References

(1) IRWIN, G. R. (1972) Characterization of part-through cracks in tension, *The Surface Crack: Physical Problems and Computational Solutions*, ASTM, New York, 1–10.

(2) *Standard test method for* J_{IC}, *a measure of fraction toughness* (1981) *ASTM E813-81*, ASTM, Philadelphia.

(3) BAUSCHKE, H.-M. and SCHWALBE, K.-H. (1991) Study of fracture behaviour of surface-cracked tensile panels of aluminum alloys, to be published.

(4) RICE, J. R. (1968) Mathematical analysis in the mechanics of fracture, *Fracture II*, (Edited by Liebowitz, H.), Academic Press, New York, pp. 191–211.

(5) McMEEKING, R. M. (1977) Finite deformation analysis of crack tip opening in elastic–plastic materials and implications for fracture, *J. Mech. Phys Solids*, **25**, 357–381.

(6) SHIH, C. F. (1981) Relationships between the *J* integral and the crack opening displacement for stationary and extending cracks, *J. Mech. Phys Solids*, **29**, 305–326.
(7) DAWES, M. G. (1976) *The application of fracture mechanics to brittle fracture in steel weld metals, PhD thesis*, (Council for National Academic Awards), The Welding Institute.
(8) NEWMAN, J. C., Jr. and RAJU, I. S. (1979) Analyses of surface cracks in finite plates under tension or bending loads, NASA Technical Paper 1578.
(9) DODDS, R. H., Jr. and READ, D. T. (1990) Experimental and numerical studies of the *J* integral for a surface flaw, *Int. J. Fracture*, **43**, 47–67.
(10) HODULAK, L. and STÖCKL, H. (1985) Bestimmung von *J*-Rißwiderstandskurven an Platten mit Oberflächenrissen, Bericht W 11/85, Fraunhofer-Institut für Werkstoffmechanik, Freiburg.
(11) BROCKS, W. and NOACK, H.-D. (1987) Elastic–plastic FEM analysis of an inner surface flaw in a pressure vessel, *Structural Mechanics in Reactor Technology* (Edited by F. H. Wittman), A. A. Balkema, Rotterdam, pp. 195–201.
(12) TRANTINA, G. G., de LORENZI, H. G., and WILKENING, W. W. (1983) Three-dimensional elastic–plastic finite element analysis of small surface cracks, *Engng Fracture Mech.*, **18**, 925–938.
(13) NIKISHKOV, G. P. and ATLURI, S. N. (1988) Three-dimensional elastic–plastic *J* integral calculations for semielliptical surface cracks in a tensile plate, *Engng Fracture Mech.*, **29**, 81–87.
(14) HELLMANN, D. and SCHWALBE, K.-H. (1984) Geometry and size effects on *J–R* and *δ–R* curves under plane stress conditions, *Fracture Mechanics: Fifteenth Symposium, ASTM STP 833*, (Edited by R. A. Sanford), ASTM, Philadelphia, pp. 577–605.
(15) SOMMER, E. (1984) *Bruchmechanische Bewertung von Oberflächenrissen*, Springer-Verlag, Berlin.
(16) HEERENS, J. (1990) Rissabstumpfung, Spaltbruch im Übergangsbereich und stabiles Risswachstum – untersucht mit den Methoden der nichtlinearen Bruchmechanik, PhD thesis, Hamburg-Harburg, University of Technology.
(17) STEENKAMP, P. A. J. M. (1986) *Investigation into the validity of J based methods for the prediction of ductile tearing and fracture*, PhD thesis, Department of Mechanical Engineering, Delft University of Technology.
(18) AURICH, D. and SOMMER, E. (1988) Effect of constraint on elastic–plastic fracture, *Steel Res.*, **59**, 358–367.
(19) KORDISCH, H. and SOMMER, E. (1988) Three-dimensional effects affecting the precision of lifetime predictions, *Fracture Mechanics: Nineteenth Symposium ASTM STP 969*, (Edited by T. A. Cruse), ASTM, Philadelphia, pp. 73–87.
(20) BROCKS, W. and KÜNECKE, G. (1988) Elastisch–plastische Bruchmechanikanalyse eines Behälters mit axialem Außenoberflächenfehler, Proceedings of the 14th MPA-Seminar, Staatliche Materialprüfungsanstalt Universität Stuttgart, Band 2, Vortrag 42.
(21) AURICH, D., BROCKS, W., JORDAN, R., OLSCHEWSKI, J., VEITH, H., and ZIEBS, J. (1983) Einfluß mehrachsiger Beanspruchungszustände auf Bruchkennwerte bei Spaltbruch im elastisch–plastischen Bereich, Proceedings of the 15th Meeting of Arbeitskreis Bruchvorgänge, Deutscher Verband für Materialforschung und -prüfung (DVM), Darmstadt, pp. 297–306.